electronics

Article

Research on Fractional-Order Global Fast Terminal Sliding Mode Control of MDF Continuous Hot-Pressing Position Servo System Based on Adaptive RBF Neural Network

Liangkuan Zhu, Xinrui Chen *, Xing Qi and Jian Zhang *

College of Mechanical and Electrical Engineering, Northeast Forestry University, Harbin 150040, China; zhulk@nefu.edu.cn (L.Z.); dach05012@nefu.edu.cn (X.Q.)
* Correspondence: xiao_km@nefu.edu.cn (X.C.); freezeman007@nefu.edu.cn (J.Z.)

Abstract: In this paper, a novel fractional-order global fast terminal sliding mode control (FGFTSMC) strategy based on an adaptive radial basis function (RBF) neural network is proposed to improve the performance of a medium density fiberboard (MDF) continuous hot-pressing position servo system with parameter perturbation and external load disturbance. Primarily, the mathematical model of the MDF continuous hot-pressing position servo system is constructed based on the dynamic equation of the hydraulic system. Then, a FGFTSMC is designed to speed up the convergence rate of the system, in which an adaptive law is used to estimate the upper bound of the unknown parameters to overcome the existing parameter perturbation of the system. In addition, an RBF neural network is introduced to approximate the external load disturbance of the system. The stability of MDF continuous hot-pressing position servo system based on the control scheme developed in this paper is proven using the Lyapunov theory. Finally, the simulation results show that the presented control scheme can effectively ensure the tracking accuracy of the system and enhance the robustness of the system.

Keywords: MDF; hot-pressing servo system; fractional-order; terminal sliding mode; adaptive law; RBF neural network

Citation: Zhu, L.; Chen, X.; Qi, X.; Zhang, J. Research on Fractional-Order Global Fast Terminal Sliding Mode Control of MDF Continuous Hot-Pressing Position Servo System Based on Adaptive RBF Neural Network. *Electronics* **2022**, *11*, 1117. https://doi.org/10.3390/electronics11071117

Academic Editor: Raffaele Carli

Received: 7 March 2022
Accepted: 28 March 2022
Published: 1 April 2022

1. Introduction

MDF is a kind of fiberboard, which is mainly made of wood fiber or other plant fiber. After adding urea formaldehyde resin or a waterproof agent, it is finally formed by high temperature, hot-pressing, and other processes, and its density is 0.65~0.80 g/cm^3 [1]. MDF has a uniform structure, low thermal expansion, smooth surface and easy to paste finish, and strong impact and bending resistance, so it is the best substitute for natural plates [2]. It is worth noting that MDF needs a wide range of raw materials, such as forest residues, sub small fuelwood, inferior boards, and surplus materials after wood processing, which significantly improves the reuse rate of forest resources. These advantages make MDF popular in wood-based panel market and greatly promote the development of the wood industry. At the same time, the expansion of market demand and the increase of economic benefits also make the development of wood-based panel in China more rapid. The technical improvement of hot-pressing process has become a key factor to improve the quality of MDF. At present, the main production equipment of MDF is continuous flat hot press, which has the advantages of continuous production process, good quality, accurate plate thick-ness and so on. At the same time, it can further improve the production efficiency and quality of MDF. The fixed thickness section in hot-pressing process directly determines the quality of MDF products, so it is necessary to ensure that the output of position servo system does not overshoot.

Electro-hydraulic servo systems are widely used in engineering due to their characteristics including high power, fast response, and high precision [3–5]. The PID method

is often used in the control of electro-hydraulic position servo systems due to its simple structure, few parameters and easy design [6]. In [7], an optimized PID algorithm is applied to motion control of micro-robots. An improved PID strategy using the beetle antenna search algorithm can effectively enhance the robustness of the drive position servo system in [8]. A PID controller designed by introducing the fuzzy adaptive algorithm can ensure that the dry battery drive system can still be effectively when the temperature is too high [9]. RBF neural networks with universal approximation properties are often used to approximate unknown parts of the system model and controller parameters [10–12]. In [13], the RBF neural network PID compound control is designed to speed up response speed of pneumatic servo system. Considering the excellent estimation characteristics of the extended state observer for disturbances. Reference [14] designed a controller with RBF neural network to adjust the PID parameters to strengthen the performance.

It is worth noting that the above literature has achieved good control results after the improvement of PID control in many aspects, but in the face of complex systems similar to [15–20], the PID controller still has problems such as low control accuracy, poor dynamic performance, and large overshoot. Fractional-order calculus may be a better solution for the deficiencies mentioned earlier. The mathematical model of fractional-order calculus can be applied to many aspects, making the dynamic response of the system more accurate, and improving the ability of dynamic system design, characterization and control [21]. At present, fractional-order has provided a new theoretical basis for the development of many fields, and has gradually been widely used in engineering [22–26]. In [24], the fractional-order PID control method is used in the hydraulic servo system of hydraulic turbine regulation, and the genetic algorithm of chaotic sequencing is adopted, so that the problem of system control parameter tuning is transformed into the problem of multi-objective optimization, and finally the overall accuracy of parameters is improved. To improve the dynamic characteristics, an idea of indirect internal model control is considered in the design of fractional order algorithms [25]. Reference [26] verified that fractional-order control strategy can significantly weaken the vibration effects of AC motors.

Sliding mode control (SMC) has broad applications such as spacecraft attitude stabilization, multiagent systems, generator load angle estimation, and unmanned surface vehicle due to its insensitivity to parameter changes [27–31]. Combining SMC with the fractional-order algorithm can take into account the advantages of both control methods, thereby improving the robustness and dynamic performance. In the latest research, fractional-order sliding mode control (FSMC) strategy has become an important research direction in many engineering fields [32–34]. In [32], a FSMC strategy is developed to reduce the ramifications of disturbances, which the nonlinear part of the system is approximated by a suitable neuro-fuzzy algorithm. In [33], when the loop gain of the hard disk drive servo system changes, the fractional-order strategy has better consistency than traditional integer order method, which is of great significance in practical applications. In [34], a FSMC method effectively improves the tracking performance of servo drive system with inherent aerodynamic loads and uncertainties, in which a fuzzy adaptive law is introduced to weaken the chattering phenomenon.

Since traditional SMC cannot ensure that the system state the rapid convergence of the system state within a limited time, some scholars have proposed the idea of terminal sliding mode control (TSMC) in recent years. In [35], a TSMC with fractional-order algorithm is developed in an underactuated mechanical system (UMS) to speed up the convergence of the system state. In Refs. [36,37], in order to solve the system affected by un-certainty and external disturbance, a fractional-order non-singular TSMC strategy is proposed to further improve the dynamic characteristics. In Refs. [38,39], the idea of backstepping is introduced into FSMC to greatly strengthen the control performance for system uncertainties.

Based on the aforementioned discussion, we propose a FGFTSMC strategy based on adaptive RBF neural network for MDF continuous hot-pressing position servo system. The contributions of this paper are summarized as follows:

(1) A FGFTSMC is constructed based on dynamics and mathematical model of the MDF hot-pressing position servo system, which ensures the rapid convergence of the system state and improves the tracking accuracy.
(2) The adaptive law and the RBF neural network are introduced to estimate the upper bound of the parameter perturbation and approximate the external load disturbance, respectively. The results of them are fed back to FGFTSMC controller to avoid system performance degradation.
(3) The Lyapunov theorem is utilized to prove the stability of system and analyze finite-time reachability of the sliding mode.

The structure of this article is as follows. The Section 2 introduces the system model and the theoretical basis of fractional-order. The Section 3 designs a FGFTSMC based on adaptive RBF neural network. The stability and finite-time convergence analysis are given in Section 4. Simulations are shown in Section 5 to illustrate the feasibility and practicality of the controller.

2. System Model and Theoretical Basis of Fractional-Order

2.1. Theoretical Basis of Fractional-Order Calculus

Fractional-order calculus is actually a kind of calculus of any order, whose order can be real or negative. ${}_{t_0}D_t^{\alpha}$ is the basic operator, t and t_0 represent the upper and lower limits of the operators, respectively. The calculus operator can be expressed as:

$$ {}_{t_0}D_t^{\alpha} = \begin{cases} \frac{d^{\alpha}}{dt^{\alpha}}, \mathrm{Re} \quad \alpha > 0, \\ 1, \quad \mathrm{Re} \quad \alpha > 0, \\ \int_{\alpha}^{t} (dv)^{(-\alpha)}, \quad \mathrm{Re} \quad \alpha > 0, \end{cases} \tag{1} $$

where α is the order of calculus.

It can be clearly seen that after introducing fractional-order operator ${}_{t_0}D_t^{\alpha}$, integral and differential can be unified. Among the many definitions of fractional calculus, Caputo type is the most practical, which is often used to solve physical problems in engineering.

Definition 1. *Ref.* [40]—*Caputo fractional-order calculus definition expression can be written uniformly*

$$ {}_{t_0}D_t^{\alpha} f(t) = \frac{1}{\Gamma(m-\alpha)} \int_{t_0}^{t} \frac{f^m(v)}{(t-v)^{\alpha-m+1}} \mathrm{d}v \tag{2} $$

where m is minimum integer not less than α and $m-1 < \alpha < m (m \in N)$ *is satisfied.*

2.2. MDF Continuous Hot-Pressing Position Servo System Model

MDF continuous piezo hydraulic position servo system consists of electro-hydraulic servo valve, servo amplifier and four-way valve control hydraulic cylinder, as shown in Figure 1. The displacement of the piston in the fixed thickness section of the hydraulic cylinder is converted into a position signal, which is compared with the given position signal to form a deviation signal input to the controller. The output of the controller converts the deviation signal into the input voltage signal and obtains the corresponding current signal through the servo amplifier to complete the motion control of the servo valve spool. Further, a certain amount of oil can enter the interior to push the piston movement, thereby driving the load to press the slab to a given thickness. The servo valve structure is shown in Figure 2.

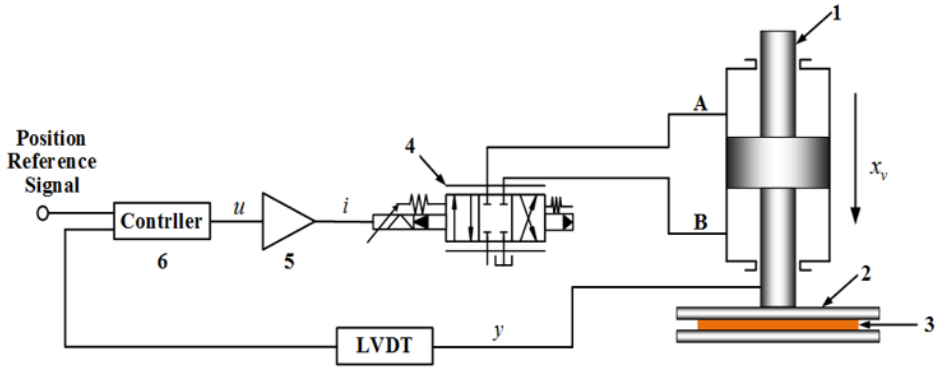

1-hydraulic cylinder piston; 2-upper pressing plate; 3-MDF slab; 4-electro-hydraulic servo valve; 5-servo amplifier; 6-controller

Figure 1. Schematic diagram of MDF plate thickness correction position servo system.

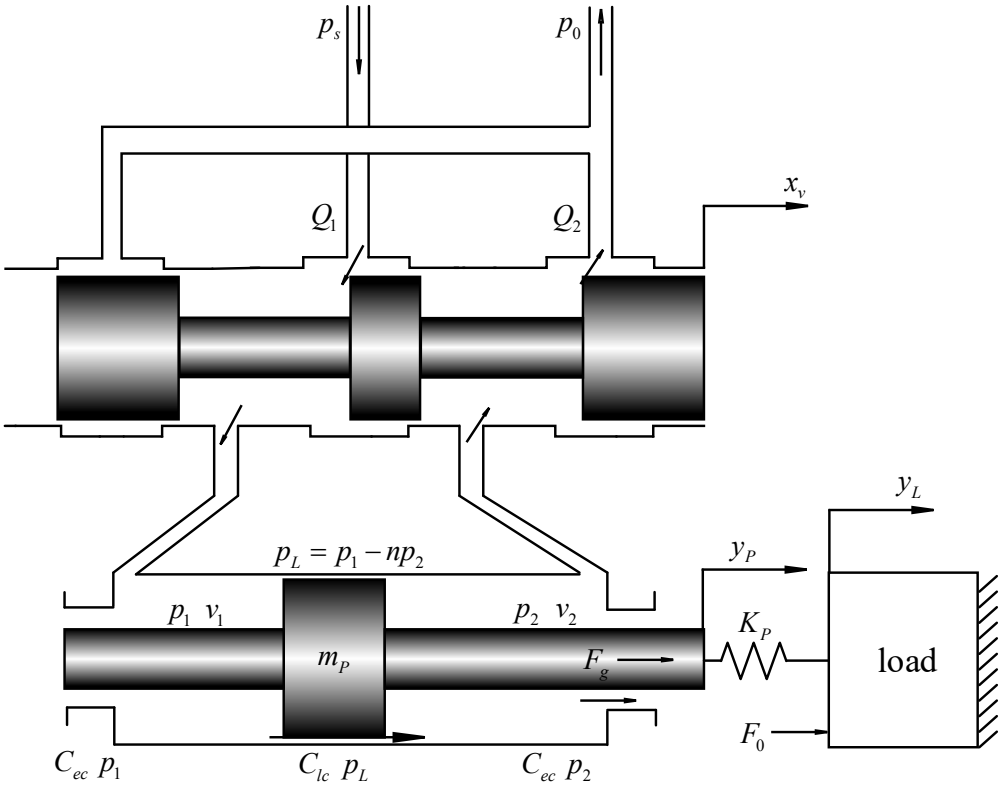

Figure 2. Structure diagram of zero opening four-way slide valve.

MDF plate thickness correction position servo system mainly adopts single four-way valve controlled symmetrical hydraulic cylinder. In this paper, taking it as the controlled object, its power mechanism is expressed by three basic equations as follows [41,42]:

$$\begin{cases} Q_L = c_d \omega x_v \sqrt{\frac{1}{\rho}(p_s - p_L \mathrm{sgn}(x_v))} \\ Q_L = A_p \frac{dy}{dt} + C_{tc} p_L + \frac{V_t}{4\beta_e} \frac{dp_L}{dt} \\ A p_L = m \frac{d^2 y}{dt^2} + B_c \frac{dy}{dt} + K_L y + F \end{cases} \tag{3}$$

where Q_L is the load flow, c_d is the flow coefficient of the slide valve, w is the area gradient of the throttle window of the slide valve, x_v is the spool displacement, ρ is the liquid density, p_s is the oil supply pressure, p_L is the load pressure, and $p_L = 2p_s/3$. A_p is the effective area of the piston, y is the displacement of the piston, C_{tc} is the total leakage coefficient; V_t

is the volume of the oil chamber of the hydraulic cylinder, β_e is the elastic modulus of the oil, m is the total mass of the load, B_c is the viscous damping coefficient, K_L is the elastic stiffness of the load, and F is the external load force.

The servo valve is approximately proportional to the servo amplifier

$$\begin{cases} k_{sv} = \frac{x_v}{i} \\ k_a = \frac{i}{u} \end{cases} \tag{4}$$

where k_{sv} is the gain of servo valve, i is the input current of servo valve, k_a is the servo amplifier gain, u is the input voltage.

Define the system variables as piston displacement, velocity and acceleration, then the state variables can be expressed as $x_1 = y$, $x_2 = \dot{y}$, $x_3 = \ddot{y}$. The output of the system is the piston displacement y, and u is the control input. According to the above analysis, the state space expression of the system can be obtained as follows:

$$\begin{cases} \dot{x}_1 = x_2 \\ \dot{x}_2 = x_3 \\ \dot{x}_3 = f(x) + g(x_v)u + D \\ y = x_1 \end{cases} \tag{5}$$

where $f(x) = a_1x_1 + a_2x_2 + a_3x_3$, $g(x_v) = a_4z(x_v)$, $z(x_v) = \sqrt{p_s - p_L\mathrm{sgn}(x_v)}$, $a_1 = -4\beta_eC_{tc}K/mV_t$, $a_2 = -K/m - 4\beta_e(A^2 + C_{tc}B_c)/mV_t$, $a_3 = -B_c/m - 4\beta_eC_{tc}/V_t$, $a_4 = 4A\beta_ec_d\omega k_{sv}k_a/mV_t\sqrt{\rho}$. $D = \Delta f(x) + \Delta g(x_v)u + d$ denotes compound disturbance composed of system parameter perturbation $\Delta f(x)$ and external load force disturbance d, and $\Delta f(x) = \Delta a_1x_1 + \Delta a_2x_2 + \Delta a_3x_3$, $d = -\dot{F}/m - (4\beta_eC_{tc}/mV_t)F$.

In the following analysis, the parameters and compound disturbance of the hot-press position servo system are considered to be both uncertain and bounded.

3. Design of FGFTSMC Controller Based on Adaptive RBF Neural Network

The structure block diagram of FGFTSMC based on adaptive RBF neural network is shown in Figure 3. Firstly, a FGFTSMC is designed for the system; secondly, the parameter perturbation and external load disturbance of the system are approximated by means of adaptive law and RBF neural network. The approximation results are fed back to the controller to strengthen robustness. Considering the weight selection of neural network, the weight adaptive law is designed.

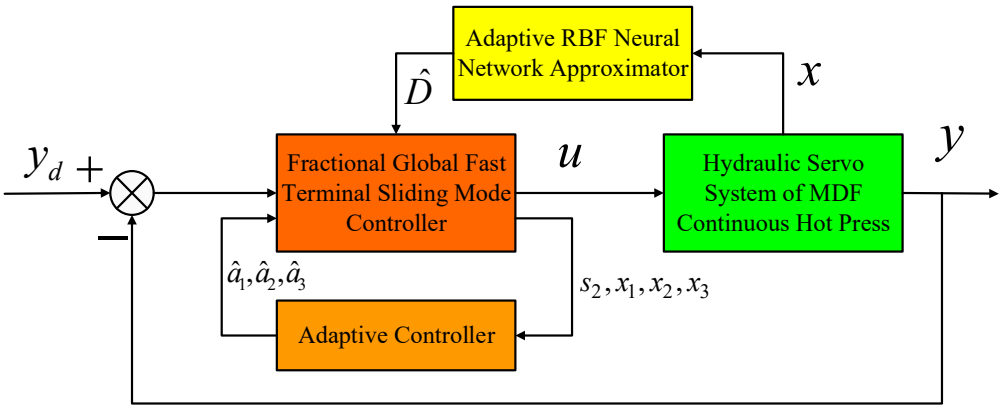

Figure 3. The structure of the FGFTSMC based on adaptive neural network approximator.

3.1. Subsection

It is assumed that the system parameters and external load disturbance are known. Considering the mathematical model of MDF continuous hot-pressing position servo system, a sliding surface is designed as follows:

$$\begin{cases} s_0 = x_1 - y_d \\ s_1 = \dot{s}_0 + \alpha_0 s_0 + \beta_0 s_0^{q_0/p_0} + c_0 \cdot D^{-\lambda} s_0 \\ s_2 = \dot{s}_1 + \alpha_1 s_1 + \beta_1 s_1^{q_1/p_1} + c_1 \cdot D^{-\lambda} s_1 \end{cases} \tag{6}$$

where y_d is desired position signal. $\alpha_0 > 0$, $\alpha_1 > 0$, $\beta_1 > 0$, $\beta_2 > 0$, p_0, p_1, q_0, q_1 is positive odd, and $q_0 < p_0$, $q_1 < p_1$. $D^{-\lambda}$ is the number order calculus operator.

For the system (5), the sliding mode control law of fractional-order global fast terminal is designed as:

$$u = -\frac{1}{g(x_v)} \left[f(x) + D + \sum_{k=0}^{1} (\bullet) + \varphi s_2 + \gamma s_2^{q/p} \right] \tag{7}$$

where $\bullet = \alpha_k s_k^{(2-k)} + \beta_k \frac{d^{2-k}}{dt^{2-k}} s_k^{q_k/p_k} + c_k \cdot D^{-\lambda+2-k} s_k$, $k = 0, 1$. $\varphi > 0$, $\gamma > 0$, $g(x_v) \neq 0$ and q, $p (q < p)$ is positive odd.

3.2. Design of Adaptive Law with Unknown Parameters

In terms of the parameter perturbation existing in the system, we design the following adaptive law:

$$\begin{cases} \dot{\hat{a}}_1 = \frac{s_2 x_1}{\rho_1} \\ \dot{\hat{a}}_2 = \frac{s_2 x_2}{\rho_2} \\ \dot{\hat{a}}_3 = \frac{s_2 x_3}{\rho_3} \end{cases} \tag{8}$$

where ρ_1, ρ_2, ρ_3 are normal number to be determined.

Thus, the control law (7) can be rewritten as:

$$u = -\frac{1}{g(x_v)} \left[\hat{f}(x) + D + \sum_{k=0}^{1} (\bullet) + \varphi s_2 + \gamma s_2^{q/p} \right] \tag{9}$$

where $\hat{f}(x) = \hat{a}_1 x_1 + \hat{a}_2 x_2 + \hat{a}_3 x_3$. The estimation error of each parameter is denoted as $\widetilde{a}_i = a_i - \hat{a}_i (i = 1, 2, 3)$.

3.3. Design of Adaptive RBF Neural Network Approximator

The structure of RBF neural network is shown in Figure 4, and for the complex disturbance in system (5), now we use the following form of RBF neural network to approximate.

$$D = \boldsymbol{W}^{*\mathrm{T}} \boldsymbol{H}(x) \tag{10}$$

$$\hat{D} = \hat{\boldsymbol{W}}^{\mathrm{T}} \boldsymbol{H}(x) \tag{11}$$

where $\hat{D}$ is estimated value of complex disturbance D, $\boldsymbol{W}^{*\mathrm{T}} = [w_1, w_2, \cdots, w_9]^{\mathrm{T}}$ is estimated value of ideal weight vector. $\boldsymbol{H}(x) = [h_1(x), h_2(x), \cdots, h_9(x)] \in \Re^9$ is the output vector of hidden layer neurons in neural network.

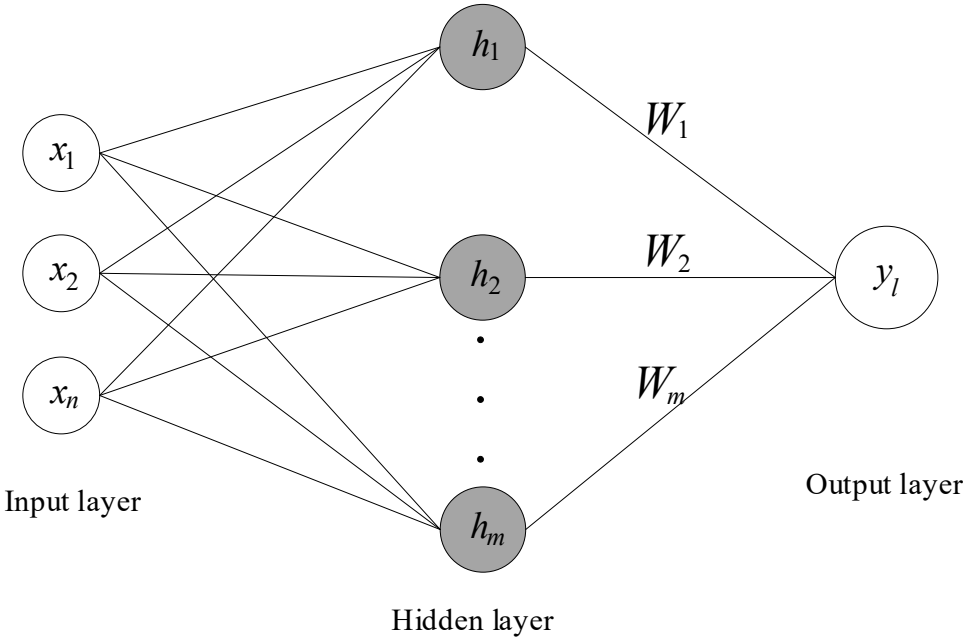

Figure 4. Structure of RBF neural network.

The Gaussian function with arbitrary derivative and radial symmetry as radial basis function does not increase the complexity of the analysis when the input is multivariate, which makes it successfully applied in many neural network control situations. Therefore, the Gaussian base function shown below is chosen as the basis function of the neural network approximator:

$$h_j(x) = \exp\left(-\|x - c_j\|^2 / 2b_j^2\right), j = 1, \cdots, 9 \tag{12}$$

where $x = [x_1, x_2, x_3]^{\mathrm{T}}$ is the state vector of the system.

In order to facilitate the stability analysis in the next section, the estimation error of neural network weight vector is defined as:

$$\widetilde{W} = \hat{W} - W^* \tag{13}$$

Therefore, the approximation error of the neural network approximator is:

$$\widetilde{D} = \hat{D} - D = \widetilde{W}^{\mathrm{T}} H(x) \tag{14}$$

However, if the weight estimation vector of neural network is not properly selected, it is easy to make the neural network approximator fall into "local optimum", which seriously affects the approximation accuracy of neural network [43]. Therefore, the adaptive law is designed as follows based on Lyapunov function

$$\dot{\hat{W}} = \eta s_2 H \tag{15}$$

where $\eta > 0$ is adjustable adaptive parameters.

Thus, the FGFTSMC law (9) can be rewritten as

$$\begin{aligned} u &= -\tfrac{1}{g(x_v)}\left[\hat{f}(x) + \hat{D} + \sum_{k=0}^{1}(\bullet) + \varphi s_2 + \gamma s_2^{q/p}\right] \\ &= -\tfrac{1}{g(x_v)}\left[\hat{f}(x) + \hat{W}^{\mathrm{T}} H + \sum_{k=0}^{1}(\bullet) + \varphi s_2 + \gamma s_2^{q/p}\right] \end{aligned} \tag{16}$$

4. Stability and Convergence Time Analysis

4.1. Stability Analysis

The tracking error of the system is fully considered and the parameters of the system are assumed to be known. The Lyapunov function is designed as follows:

$$V_1 = \frac{1}{2}s_2^2 \tag{17}$$

The derivation of V_1 can be expressed as:

$$\dot{V}_1 = s_2\dot{s}_2 \ = s_2[f(x) + g(x_v)u + D + \sum_{k=0}^{1}(\bullet)] \tag{18}$$

By substituting the control law (7) into the above equation, we can get the following results

$$\dot{V}_1 = -\varphi s_2^2 - \gamma s_2^{(q+p)/p} \tag{19}$$

Since $\varphi > 0$, $\gamma > 0$, and $p + q$ is an even number, $\dot{V}_1 \leq 0$ can be guaranteed and the system is stable.

Considering the actual situation, Lyapunov function is designed to be based on the unknown parameters and external load interference in the system

$$V = V_1 + \sum_{i=1}^{3}\frac{1}{2}\rho_i\widetilde{a}_i^2 + \frac{1}{2\eta}\widetilde{W}^{\mathrm{T}}\widetilde{W} \tag{20}$$

The derivation of Equation (20) can be obtained as follows:

$$\dot{V} = s_2\dot{s}_2 + \sum_{i=1}^{3}\rho_i\widetilde{a}_i\dot{\widetilde{a}} + \frac{1}{\eta}\widetilde{W}^{\mathrm{T}}\dot{\widetilde{W}} \tag{21}$$

Then

$$\begin{aligned}\dot{V} \ &= s_2\dot{s}_2 + \sum_{i=1}^{3}\rho_i\widetilde{a}_i\dot{\widetilde{a}} + \tfrac{1}{\eta}\widetilde{W}^{\mathrm{T}}\dot{\widetilde{W}} \\ &= s_2[f(x) + g(x_v)u + D + \sum_{k=0}^{1}(\bullet)] + \sum_{i=1}^{3}\rho_i\widetilde{a}_i\dot{\widetilde{a}} + \tfrac{1}{\eta}\widetilde{W}^{\mathrm{T}}\dot{\widetilde{W}}\end{aligned} \tag{22}$$

Since $\widetilde{a}_i = a_i - \hat{a}_i$, $\dot{\widetilde{a}}_i = -\dot{\hat{a}}_i$. Considering the adaptive law (8) and the control law (16), Equation (22) can be rewritten as

$$\begin{aligned}\dot{V} \ &= s_2\dot{s}_2 + \sum_{i=1}^{3}\rho_i\widetilde{a}_i\dot{\widetilde{a}} + \tfrac{1}{\eta}\widetilde{W}^{\mathrm{T}}\dot{\widetilde{W}} \\ &= s_2[f(x) + g(x_v)u + D + \sum_{k=0}^{1}(\bullet)] \ - \sum_{i=1}^{3}\rho_i\widetilde{a}_i\dot{\hat{a}} + \tfrac{1}{\eta}\widetilde{W}^{\mathrm{T}}\dot{\widetilde{W}} \\ &= s_2[\sum_{i=1}^{3}\widetilde{a}_i x_i + D - \hat{W}^{\mathrm{T}}H] - \sum_{i=1}^{3}\rho_i\widetilde{a}_i\dot{\hat{a}} + \tfrac{1}{\eta}\widetilde{W}^{\mathrm{T}}\dot{\widetilde{W}} + s_2[-\varphi s_2 - \gamma s_2^{q/p}]\end{aligned} \tag{23}$$

where $\sum_{k=1}^{3}\widetilde{a}_i x_i = f(x) - \hat{f}(x)$.

According to Equation (13), we have

$$\dot{\widetilde{W}} = \dot{\hat{W}} - \dot{W}^{*} = \dot{\hat{W}} \tag{24}$$

Substituting the Equations (10), (15), (16) and (24) into Equation (23), we can obtain

$$\begin{aligned}\dot{V} &= s_2[W^{*\mathrm{T}}H - \hat{W}^{\mathrm{T}}H] + \tfrac{1}{\eta}\widetilde{W}^{\mathrm{T}}\dot{\widetilde{W}} + s_2[-\varphi s_2 - \gamma s_2^{q/p}] \\ &= \widetilde{W}^{\mathrm{T}}[\tfrac{1}{\eta}\dot{\hat{W}} - s_2 H] + s_2[-\varphi s_2 - \gamma s_2^{q/p}] \\ &= -\varphi s_2^2 - \gamma s_2^{(q+p)/p}\end{aligned} \tag{25}$$

As mentioned above $\varphi > 0$, $\gamma > 0$, it can be obtained that $\dot{V} \leq 0$. Therefore, the proposed control scheme can ensure the asymptotic stability of the closed-loop MDF hot-pressing position servo system.

4.2. Analysis of Convergence Time

Assuming that the effects of unknown parameters of the system are ignored, it can be obtained from Equation (6)

$$\dot{s}_2 = \ddot{s}_1 + \alpha_1\dot{s}_1 + \beta_1\frac{\mathrm{d}}{\mathrm{dt}}s_1^{q_1/p_1} + c_1 \cdot D^{-\lambda}s_1 \tag{26}$$

Since $s_i = \dot{s}_{i-1} + \alpha_{i-1}s_{i-1} + \beta_{i-1}s_{i-1}^{q_{i-1}/p_{i-1}} + c_{i-1} \cdot D^{-\lambda}s_{i-1}$, $i = 1, 2$. Then the j-th derivative of s_i is

$$s_i^{(j)} = s_{i-1}^{(j+1)} + \alpha_{i-1}s_{i-1}^{(j)} + \beta_{i-1}\frac{\mathrm{d}^j}{\mathrm{dt}^j}s_{i-1}^{q_{i-1}/p_{i-1}} + c_{i-1} \cdot D^{j-\lambda}s_{i-1} \tag{27}$$

Then the second order of s_i can be expressed as

$$\ddot{s}_1 = \dddot{s}_0 + \alpha_0\ddot{s}_0 + \beta_0\frac{\mathrm{d}^2}{\mathrm{dt}^2}s_0^{q_0/p_0} + c_0 \cdot D^{2-\lambda}s_0 \tag{28}$$

Therefore, it can be deduced from Equation (27)

$$\begin{aligned}\dot{s}_2 &= \dddot{x}_1 + \alpha_0\ddot{s}_0 + \alpha_1\dot{s}_1 + \beta_0\tfrac{\mathrm{d}^2}{\mathrm{dt}^2}s_0^{q_0/p_0} + \beta_1\tfrac{\mathrm{d}}{\mathrm{dt}}s_1^{q_1/p_1} + c_0 \cdot D^{2-\lambda}s_0 + c_1 \cdot D^{1-\lambda}s_1 \\ &= \dot{x}_3 + \alpha_0\ddot{s}_0 + \alpha_1\dot{s}_1 + \beta_0\tfrac{\mathrm{d}^2}{\mathrm{dt}^2}s_0^{q_0/p_0} + \beta_1\tfrac{\mathrm{d}}{\mathrm{dt}}s_1^{q_1/p_1} + c_0 \cdot D^{2-\lambda}s_0 + c_1 \cdot D^{1-\lambda}s_1\end{aligned} \tag{29}$$

By substituting the control law (7) into the above equation, we can obtain

$$\dot{s}_2 = -(\varphi s_2 + \gamma s_2^{q/p}) \tag{30}$$

By solving the differential Equation (30) above, we can get the initial state of the sliding mode $s_2(0) \neq 0$ the time to converge $s_2(t) = 0$ to equilibrium is

$$t_{s_2} = \frac{p}{\varphi(p-q)}\ln\frac{\varphi(s_2(0))^{(p-q)/p} + \gamma}{\gamma} \tag{31}$$

5. Simulation Analysis

In this section, three simulation experiments will be designed under the matlab2016b simulation platform to evaluate applicability of developed scheme. Before simulation experiment, the following assumptions should be satisfied:

(1) The initial state is $x_1(0) = x_2(0) = x_3(0) = 0$.
(2) The reference output signal is $y_d = 0.1$ mm .
(3) The disturbance of unknown external load force is $d(t) = 54,780 + 4000\sin(4\pi t)$.

According to the above assumptions, the initial error $e(0) = x_1(0) - y_d(0) = -0.1 \text{ mm} < 0$. The nominal values of system parameters are shown in Table 1.

Table 1. Nominal values of hydraulic servo system parameters.

Physical Parameter	Numerical Value	Physical Parameter	Numerical Value
K_{sv}	0.01	C_{tc}	5
K_a	0.0125	p_s	25
c_d	0.61	B_c	6.85
ρ	850	K	2.4
A	0.1256	V_t	2.356
ω	0.025	m	1000
β_e	6.85	-	-

Case 1: In this part, a comparative experiment is established to explore the advantages of the FGFTSMC law (16) presented in this paper compared with the adaptive sliding mode control (ASMC) method and the traditional SMC strategy.

The parameters selection of FGFTSMC method are $c_0 = c_1 = 15$, $\lambda = 0.8$, $\alpha_0 = \alpha_1 = 200$, $\beta_0 = \beta_1 = 1 \times 10^{-10}$, $\varphi = 13,000$, $\gamma = 1600$, $p_0 = p_1 = 9$, , $q_0 = q_1 = 1$, $p = 5$, $q = 3$.

The parameters of the ASMC are designed as follows: $c_2 = 1 \times 10^4$, $\eta = 100$, $c_1 = 400$, $\rho_1 = 1 \times 10^{-6}$, $\rho_2 = 1 \times 10^{-7}$, $\rho_3 = 1 \times 10^{-5}$.

The parameters of SMC are designed as: $c_1 = 400$, $c_2 = 1 \times 10^4$, $\eta = 70$.

The simulation results are shown in Figures 5 and 6.

It can be clearly seen from Figure 5 that the FGFTSMC method is much faster in response speed than the ASMC and SMC. At around 0.05 s, the FGFTSMC can track the desired signal and keep it stable, while the adaptive sliding mode controller lags far behind in speed, which fully verifies that the designed controller has better convergence effect. Figure 6 clearly shows that the convergence speed of the FGFTSMC designed in this paper is much faster than ASMC and SMC. Although the designed method is higher than ASMC and SMC in terms of control input, its control input is still within a reasonable range. Both Figures 5 and 6 demonstrate well the feasibility and effectiveness of the controller design.

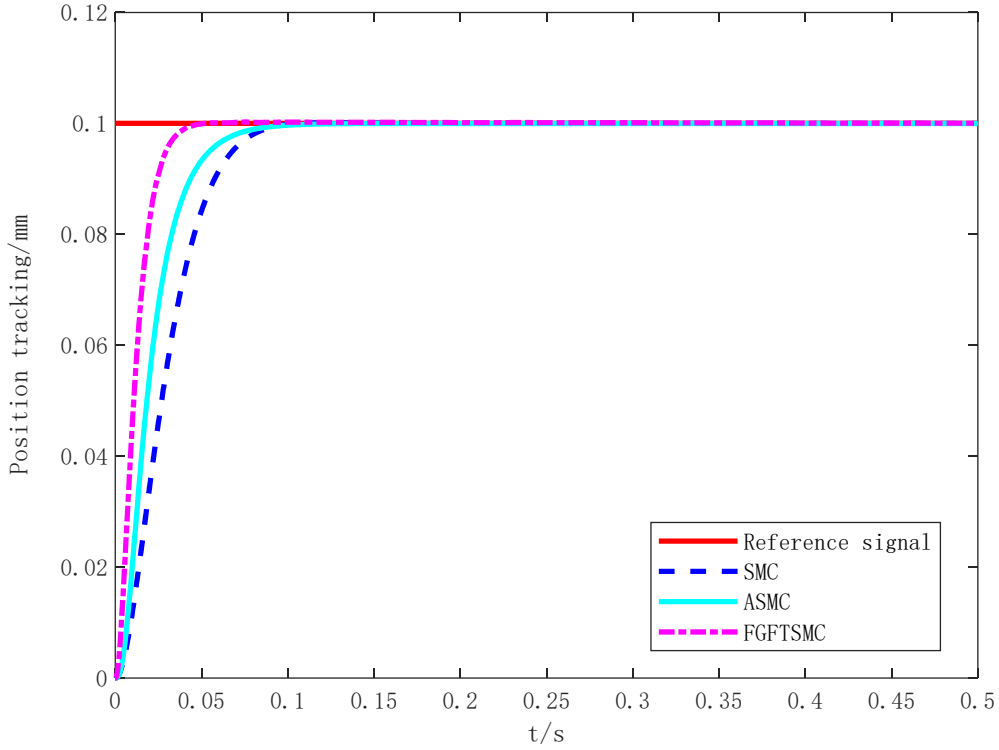

Figure 5. Comparison of position tracking curves.

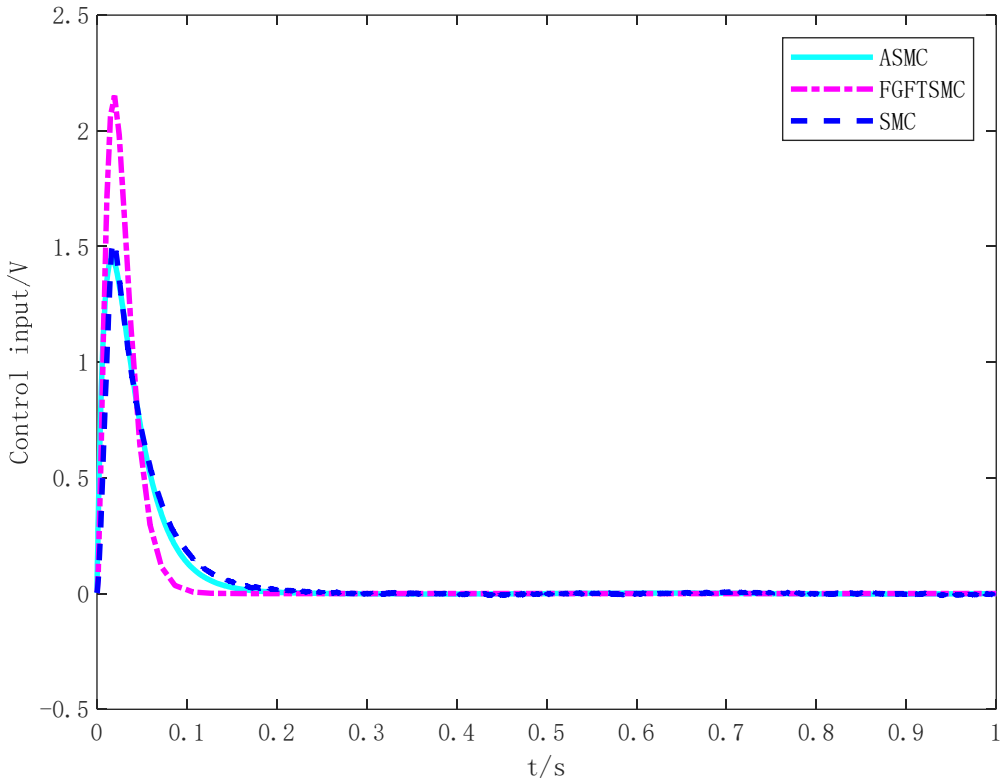

Figure 6. Control output comparison.

Case 2: To further confirm fast convergence of controller (16) in tracking dynamic signals, the given signal is chosen as $y_d = 0.5\cos(10\pi t)mm$, and the controller parameters are designed as: $\alpha_0 = 150$, $\alpha_1 = 100$, $p = 5$, $q = 3$, $p_0 = p_1 = 9$, $q_0 = q_1 = 1$, $\varphi = 1000$, $\theta = 2000$, $\rho_1 = 1 \times 10^{-12}$, $\rho_2 = 1 \times 10^{-13}$, $\rho_3 = 1 \times 10^{-6}$, $\lambda = 0.75$, $c_1 = c_2 = 10$, $\beta_0 = \beta_1 = 1 \times 10^{-15}$.

The simulation results are shown in Figures 7–9.

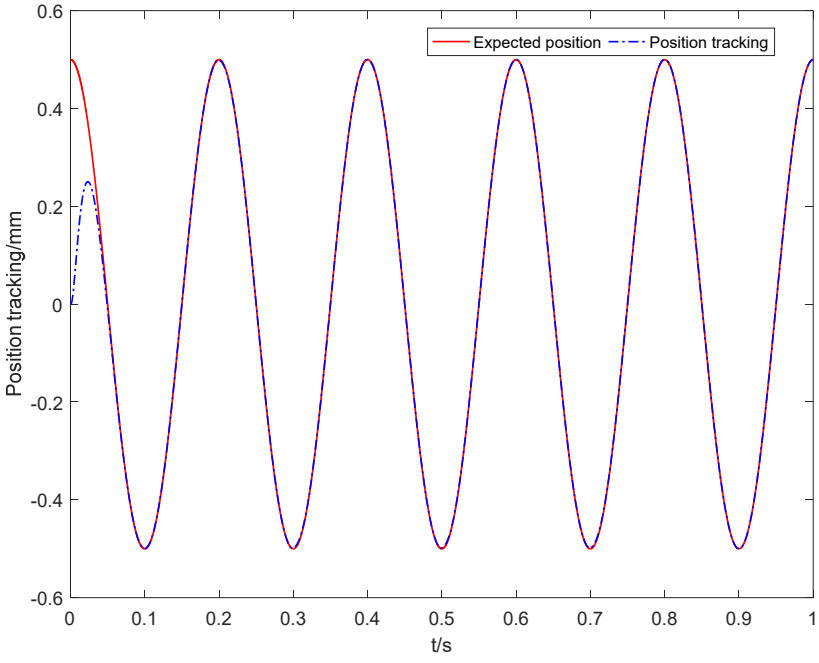

Figure 7. Position tracking curve under dynamic signal.

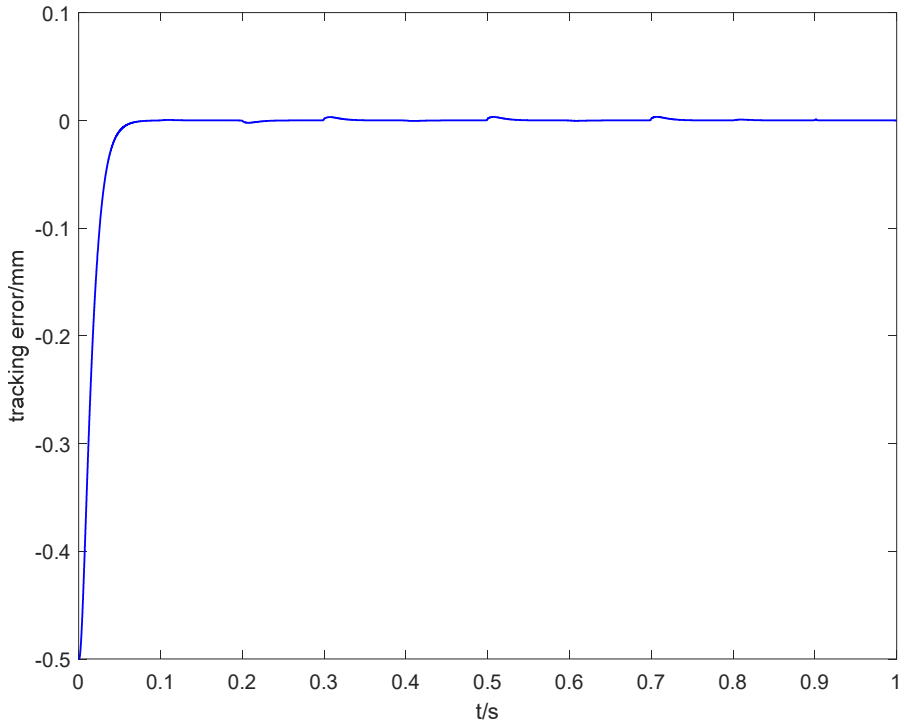

Figure 8. Tracking error curve.

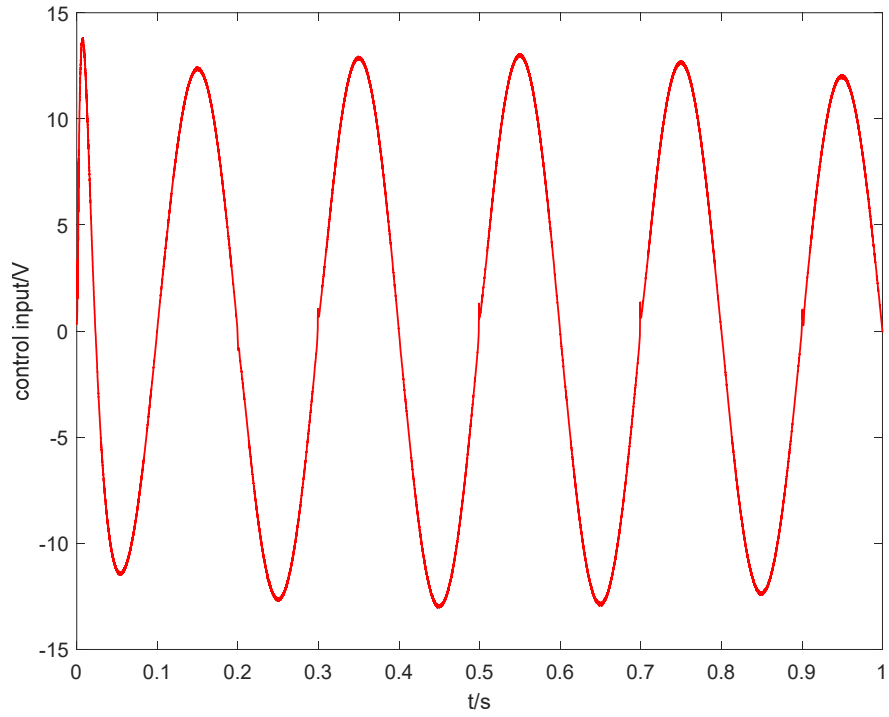

Figure 9. System control input curve.

Figures 7 and 8 further illustrate that the FGFTSMC can still achieve fast and accurate control when tracking the dynamic position signal, and its convergence time is about 0.05121 s. From Figure 9, the output signal of the control law is relatively stable without obvious chattering, which indicates that this method can promote the robustness.

Case 3: Compared with the PID controller and the SMC, it is verified that the RBF neural network has an accurate estimation effect and the control law (16) still has a good

control performance for the system in the face of compound disturbance. The control parameters of the controller are chosen as follows:

The relevant parameters of the adaptive RBF neural network approximator are selected as follows: $c_j = 10^4 \times [-8\ -6\ -4\ -2\ 0\ 2\ 4\ 6\ 8]$, $b_j = 100$, $j = 1, 2, 3$. The adaptive gain selection of neural network weight vector is $\eta = 2 \times 10^7$.

The parameters of the FGFTSMC are chosen as: $\lambda = 0.75$, $\alpha_0 = \alpha_1 = 200$, $\beta_0 = \beta_1 = 1 \times 10^{-10}$, $p_0 = p_1 = 9$, $q_0 = q_1 = 1$, $c_0 = c_1 = 15$, $p = 5$, $q = 3$, $\varphi = 13,000$, $\gamma = 1600$.

The adaptive parameters are $\rho_1 = 1 \times 10^{-8}$, $\rho_2 = 1 \times 10^{-10}$, $\rho_3 = 5 \times 10^{-8}$.

The simulation results are shown in Figures 10–14.

Figure 10 shows the output and approximation error of the system interference and adaptive RBF neural network approximator. The designed neural network approximator and composite interference have basically no error under the appropriate neural network parameters, which proves that it has a very superior approximation ability. This will further strengthen the robustness of the FGFTSMC.

Figure 11 shows the position tracking of the three controllers. Compared with PID algorithm and SMC, the FGFTSMC can track the reference signal faster. From the partial enlarged image that the FGFTSMC can achieve accurate position tracking without overshoot, and has a small tracking error after the system is stabilized. Compared with the PID method, although FGFTSMC has no obvious advantages in tracking error, its response speed is significantly faster than that of the PID controller. Therefore, the FGFTSMC can track the input reference signal precisely when there are unknown parameters and disturbances in the system and effectively improve the steady-state and transient performance.

Figure 12 shows the control input signal curve of three controllers. Compared with the SMC and PID strategies, the FGFTSMC control input initial signal is larger but shorter convergence time. This proves that FGFTSMC has good convergence.

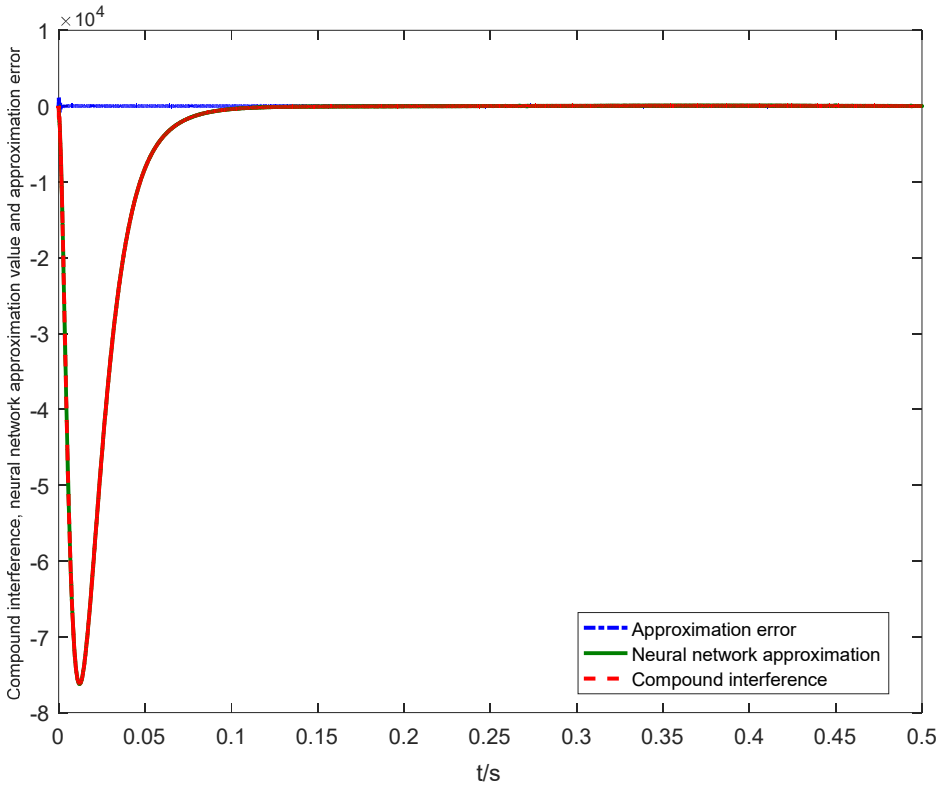

Figure 10. System disturbance term and output and approximation error of neural network approximator.

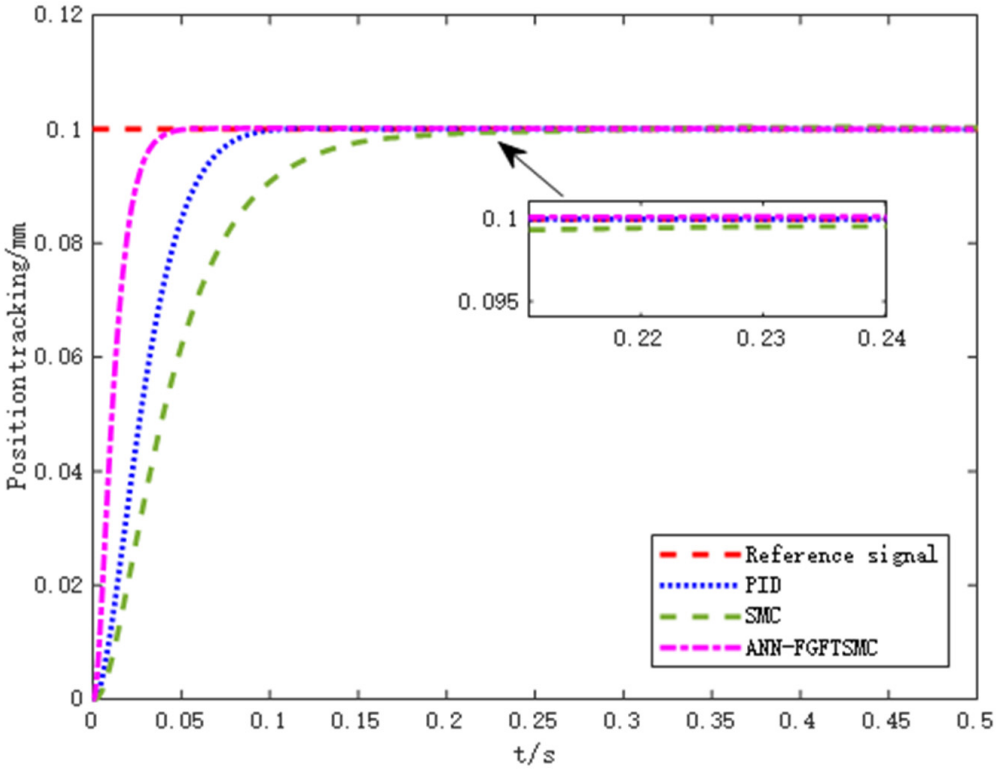

Figure 11. Position tracking curve.

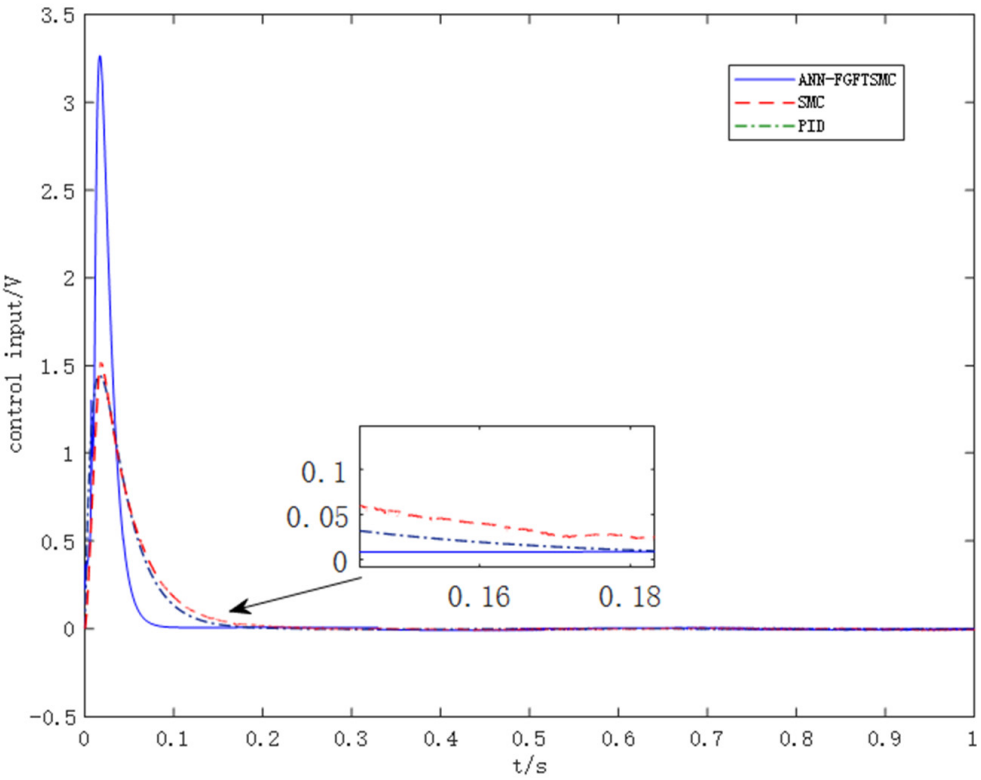

Figure 12. Control input curves of three controllers.

Figure 13 is an estimation curve of unknown parameters of the system. The adaptive law designed is shown by Figure 13a–c, respectively, for unknown parameters, and

estimated value in the system. It can be clearly seen that the adaptive law can effectively estimate the upper bound of the model unknown parameters.

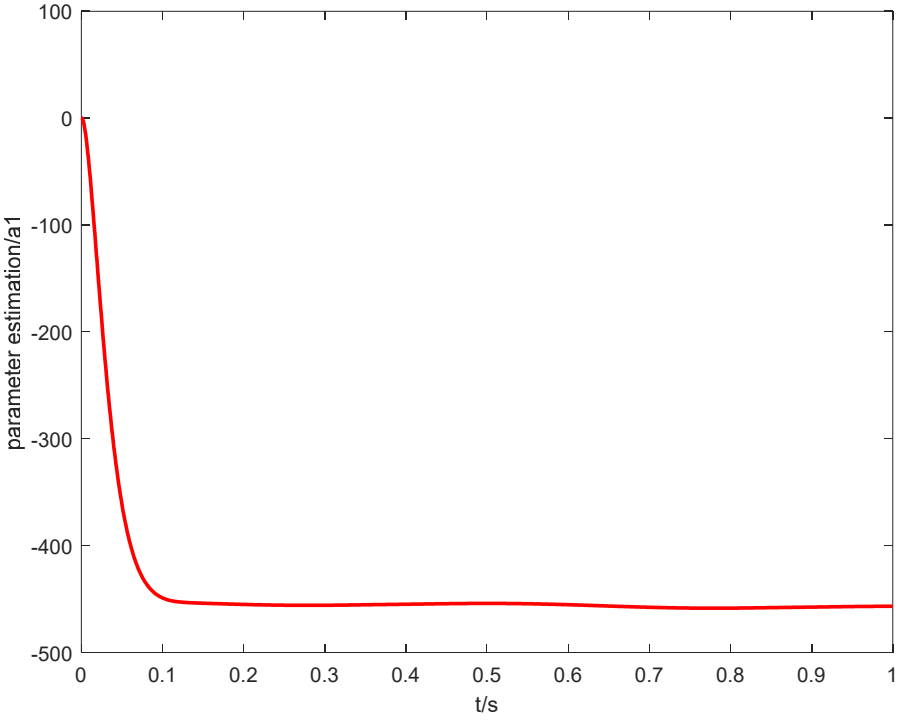

(**a**)

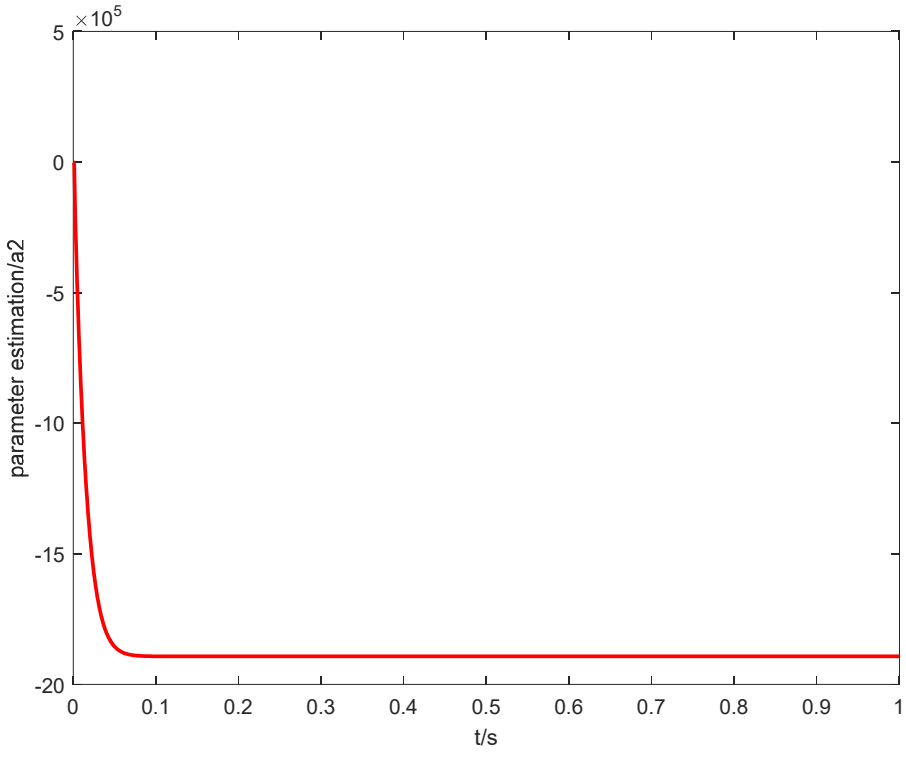

(**b**)

Figure 13. *Cont.*

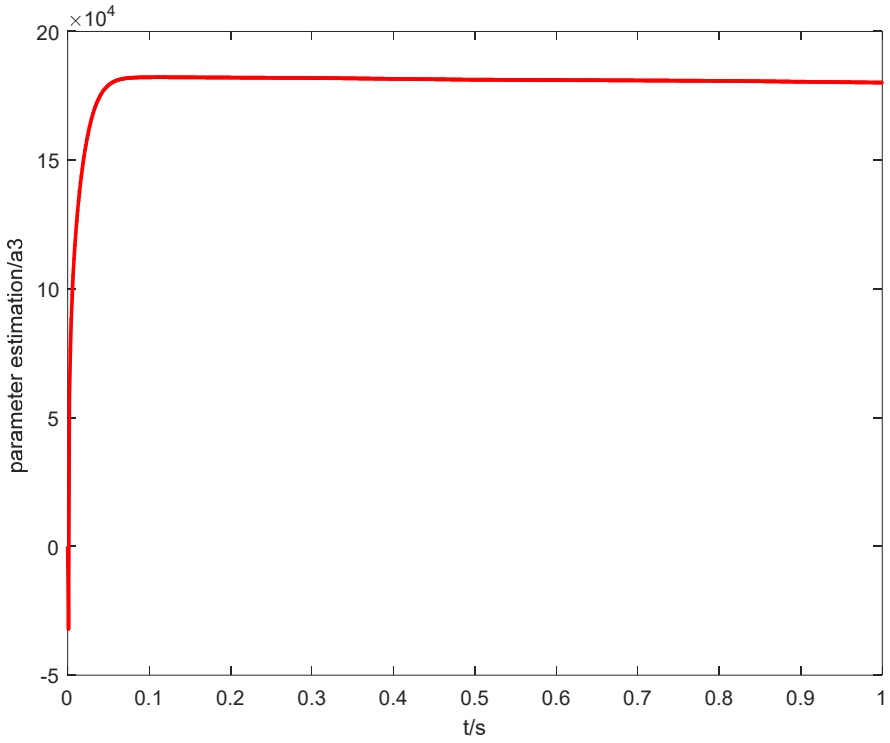

(**c**)

Figure 13. (**a**) Estimation of system parameter a_1, (**b**) estimation of system parameter a_2, and (**c**) Estimation of system parameter a_3.

Figure 14 is the change curve of sliding mode in FGFTSMC. It can be found that the sliding mode surface can converge quickly, which verifies that the control strategy has excellent control performance.

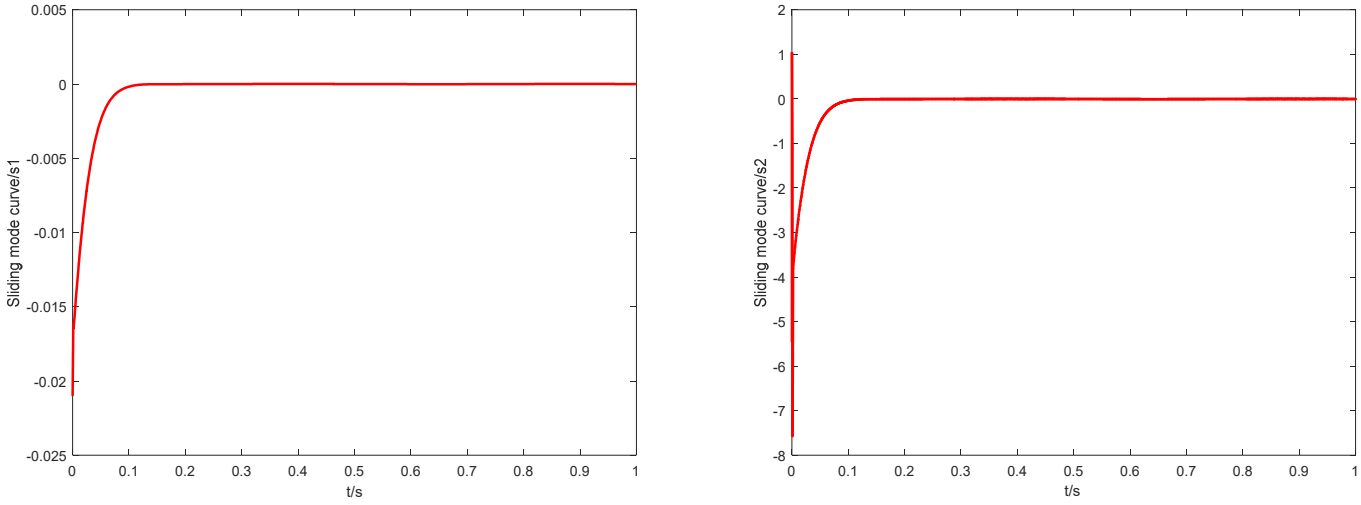

(**a**) (**b**)

Figure 14. Sliding mode change curve. (**a**) The change curve of s_1; (**b**) The change curve of s_2.

Similar with simulation case 1, Figures 10–14 show that the FGFTSMC strategy still has good control performance after considering unknown parameters and interference of the system, which shows that the control algorithm has excellent compatibility.

6. Conclusions

For the problems of parameter perturbation and load disturbance in MDF continuous hot-pressing position servo systems, a FGFTSMC strategy based on adaptive RBF neural network is designed. Firstly, the FGFTSMC control law is designed by selecting the appropriate sliding mode surface, and the adaptive law is introduced to estimate the upper bound of the unknown parameters of the model. Secondly, the disturbance is approximated with the aid of the weight adaptively adjusted RBF neural network. Finally, the result of the approximate disturbance is applied to the FGFTSMC for compensation. It is verified by simulation that the designed control method can approximate well the external load disturbance and effectively improve the tracking accuracy and robustness of the system. Considering the limitations of the proposed scheme in case of system control gain is known, we will focus on exploring the improved algorithm under the time-varying control gain in future research. In addition, the performance test of the proposed algorithm on the real platform will also be implemented.

Author Contributions: Conceptualization, L.Z.; formal analysis, X.C.; writing-original draft preparation, X.Q. and J.Z.; review and editing, L.Z., X.C., X.Q. and J.Z. All authors have read and agreed to the published version of the manuscript.

Funding: This research was funded by the National Key Research and Development Program of China (Grant No. 2020YFB2009902), Fundamental Research Funds of Central Universities (2572018BF02), National Natural Science Foundation of China (31370710), the 948 Project from the Ministry of Forestry of China (2014-4-46), Construction project of all English teaching courses for graduate students of Northeast Forestry University.

Acknowledgments: The authors thank the anonymous reviewers for their useful comments that improved the quality of the paper.

Conflicts of Interest: The authors declare no conflict of interest.

References

1. Lin, W. Current situation of MDF Industry and analysis of product quality. *Sichuan Build. Mater.* **2017**, *43*, 217–218.
2. Ren, R. Analysis on quality problems of MDF products. *Hebei Enterp.* **2015**, *8*, 143–144.
3. Li, G.; Ding, Y.; Feng, Y.; Li, Y. AMESim simulation and energy control of hydraulic control system for direct drive electro-hydraulic servo die forging hammer. *Int. J. Hydromechatron.* **2019**, *2*, 203–225. [CrossRef]
4. Wiens, T. Engine speed reduction for hydraulic machinery using predictive algorithms. *Int. J. Hydromechatron.* **2019**, *2*, 16–31. [CrossRef]
5. Togawa, T.; Tachibana, T.; Tanaka, Y.; Peng, J. Hydro-disk-type of electrorheological brakes for small mobile robots. *Int. J. Hydromechatron.* **2021**, *4*, 99–115. [CrossRef]
6. Wang, L. *PID Control System Design and Automatic Tuning Using MATLAB/Simulink*; Wiley-IEEE Press Ltd.: Chichester, UK, 2020; pp. 1–30.
7. Karami, M.; Tavakolpour-Saleh, A.R.; Norouzi, A. Optimal Nonlinear PID Control of a Micro-Robot Equipped with Vibratory Actuator Using Ant Colony Algorithm: Simulation and Experiment. *J. Intell. Robot. Syst.* **2020**, *99*, 773–796. [CrossRef]
8. Fan, Y.; Shao, J.; Sun, G. Optimized PID Controller Based on Beetle Antennae Search Algorithm for Electro-Hydraulic Position Servo Control System. *Sensors* **2019**, *19*, 2727. [CrossRef]
9. Caglar, C.; Mustafa, K. Fuzzy self-adaptive PID control technique for driving HHO dry cell systems. *Int. J. Hydrogen Energy* **2020**, *45*, 26059–26069.
10. Wang, B.; Jahanshahi, H.; Volos, C.; Bekiros, S.; Aly, A.A. A New RBF Neural Network-Based Fault-Tolerant Active Control for Fractional Time-Delayed Systems. *Electronics* **2021**, *10*, 1501. [CrossRef]
11. Al-Darraji, I.; Piromalis, D.; Kakei, A.A.; Khan, F.Q.; Stojmenovic, M.; Tsaramirsis, G.; Papageorgas, P.G. Adaptive robust controller design-based rbf neural network for aerial robot arm model. *Electronics* **2021**, *10*, 831. [CrossRef]
12. Lopac, N.; Jurdana, I.; Lerga, J.; Wakabayashi, N. Particle-Swarm-Optimization-Enhanced Radial-Basis-Function-Kernel-Based Adaptive Filtering Applied to Maritime Data. *J. Mar. Sci. Eng.* **2021**, *9*, 439. [CrossRef]
13. Luo, J.; Yuan, R.; Yuan, Y.; Ba, S.; Zhang, Z. Analysis of Speed Servo System of Pneumatic Manipulator Based RBF Neural Network PID Control. *Appl. Mech. Mater.* **2010**, *41*, 65–70. [CrossRef]

14. Liu, C.; Wang, M.; Zhang, J. Research on RBF Neural Network PID Controller for Quadcopter ESO. *Electro-Opt. Control.* **2021**, *28*, 84.
15. Meda-Campaña, J.A.; Escobedo-Alva, J.O.; Rubio, J.D.J.; Aguilar-Ibañez, C.; Perez-Cruz, J.H.; Obregon-Pulido, G.; Tapia-Herrera, R.; Orozco, E.; Cordova, D.A.; Islas, M.A. On the Rejection of Random Perturbations and the Tracking of Random References in a Quadrotor. *Complexity* **2022**, *2022*, 1–16. [CrossRef]
16. de Jesús Rubio, J.; Orozco, E.; Cordova, D.A.; Islas, M.A.; Pacheco, J.; Gutierrez, G.J.; Zacarias, A.; Soriano, L.A.; Meda-Campaña, J.A.; Mujica-Vargas, D. Modified Linear Technique for the Controllability and Observability of Robotic Arms. *IEEE Access* **2022**, *10*, 3366–3377. [CrossRef]
17. Aguilar-Ibanez, C.; Moreno-Valenzuela, J.; García-Alarcón, O.; Martinez-Lopez, M.; Acosta, J.Á.; Suarez-Castanon, M.S. PI-Type Controllers and Σ–Δ Modulation for Saturated DC-DC Buck Power Converters. *IEEE Access* **2021**, *9*, 20346–20357. [CrossRef]
18. Soriano, L.A.; Rubio, J.D.J.; Orozco, E.; Cordova, D.A.; Ochoa, G.; Balcazar, R.; Cruz, D.R.; Meda-Campaña, J.A.; Zacarias, A.; Gutierrez, G.J. Optimization of Sliding Mode Control to Save Energy in a SCARA Robot. *Mathematics* **2021**, *9*, 3160. [CrossRef]
19. Soriano, L.A.; Zamora, E.; Vazquez-Nicolas, J.M.; Hernández, G.; Barraza Madrigal, J.A.; Balderas, D. PD control compensation based on a cascade neural network applied to a robot manipulator. *Front. Neurorobot.* **2020**, *78*, 1–9. [CrossRef]
20. Silva-Ortigoza, R.; Hernández-Márquez, E.; Roldán-Caballero, A.; Tavera-Mosqueda, S.; Marciano-Melchor, M.; García-Sánchez, J.R.; Hernández-Guzmán, V.M.; Silva-Ortigoza, G. Sensorless Tracking Control for a "Full-Bridge Buck Inverter–DC Motor" System: Passivity and Flatness-Based Design. *IEEE Access* **2021**, *9*, 132191–132204. [CrossRef]
21. Kishore, B.; Rosdiazli, I.; Mohd, N.; Sabo, M.; Vivekananda, R. *Fractional-Order Systems and PID Controllers*; Springer: Berlin, Germany, 2020; pp. 1–20.
22. Agila, A.; Baleanu, D.; Eid, R.; Irfanoglu, B. A freely damped oscillating fractional dynamic system modeled by fractional Euler–Lagrange equations. *J. Vib. Control* **2018**, *24*, 1228–1238. [CrossRef]
23. Delavari, H.; Senejohnny, D.; Baleanu, D. Sliding observer for synchronization of fractional order chaotic systems with mismatched parameter. *Open Phys.* **2012**, *10*, 1095–1101. [CrossRef]
24. Chen, Z.; Yuan, X.; Ji, B.; Wang, P.; Tian, H. Design of a fractional order PID controller for hydraulic turbine regulating system using chaotic non-dominated sorting genetic algorithm II. *Energy Convers. Manag.* **2014**, *84*, 390–404. [CrossRef]
25. Trivedi, R.; Padhy, P.K. Design of Indirect Fractional Order IMC Controller for Fractional Order Processes. *IEEE Trans. Circuits Syst. II Express Briefs* **2020**, *68*, 968–972. [CrossRef]
26. Zhao, H.; Li, D.; Deng, W.; Yang, X. Research on Vibration Suppression Method of Alternating Current Motor Based on Fractional Order Control Strategy. *Proc. Inst. Mech. Eng. Part E J. Process Mech. Eng.* **2017**, *231*, 786–799. [CrossRef]
27. Liu, Y.; Jiang, B.; Lu, J.; Cao, J.; Lu, G. Event-triggered sliding mode control for attitude stabilization of a rigid spacecraft. *IEEE Trans. Syst. Man Cybern. Syst.* **2018**, *50*, 3290–3299. [CrossRef]
28. Liu, H.; Cheng, L.; Tan, M.; Hou, Z.G. Exponential finite-time consensus of fractional-order multiagent systems. *IEEE Trans. Syst. Man Cybern. Syst.* **2018**, *50*, 1549–1558. [CrossRef]
29. Wang, H.; Liu, P.X.; Zhao, X.; Liu, X. Adaptive fuzzy finite-time control of nonlinear systems with actuator faults. *IEEE Trans. Cybern.* **2019**, *50*, 1786–1797. [CrossRef]
30. Lopac, N.; Bulic, N.; Vrkic, N. Sliding mode observer-based load angle estimation for salient-pole wound rotor synchronous generators. *Energies* **2019**, *12*, 1609. [CrossRef]
31. Qiu, B.; Wang, G.; Fan, Y.; Mu, D.; Sun, X. Adaptive sliding mode trajectory tracking control for unmanned surface vehicle with modeling uncertainties and input saturation. *Appl. Sci.* **2019**, *9*, 1240. [CrossRef]
32. Song, S.; Zhang, B.; Xia, J.; Zhang, Z. Adaptive Backstepping Hybrid Fuzzy Sliding Mode Control for Uncertain Fractional-Order Nonlinear Systems Based on Finite-Time Scheme. *IEEE Trans. Syst. Man Cybern. Syst.* **2020**, *50*, 1559–1569. [CrossRef]
33. Ying, L.; Tao, Z.; Lee, B.J.; Kang, C.; Chen, Y. Fractional-Order Proportional Derivative Controller Synthesis and Implementation for Hard-Disk-Drive Servo System. *IEEE Trans. Control. Syst. Technol.* **2014**, *22*, 281–289.
34. Ullah, N.; Shao, W.; Khattak, M.I.; Shafi, M. Fractional order adaptive fuzzy sliding mode controller for a position servo system subjected to aerodynamic loading and nonlinearities. *Aerosp. Sci. Technol.* **2015**, *43*, 381–387. [CrossRef]
35. Trieu, P.V.; Cuong, H.M.; Dong, H.Q.; Tuan, N.H.; Le, A.T. Adaptive fractional-order fast terminal sliding mode with fault-tolerant control for underactuated mechanical systems: Application to tower cranes. *Autom. Constr.* **2021**, *123*, 103533. [CrossRef]
36. Aghaeinezhad, S.M.; Taghizadeh, M.; Mazare, M.; Kazemi, M. Individual Pitch Angle Control of a Variable Speed Wind Turbine Using Adaptive Fractional Order Non-Singular Fast Terminal Sliding Mode Control. *Int. J. Precis. Eng. Manuf.* **2021**, *22*, 511–522. [CrossRef]
37. Labbadi, M.; Cherkaoui, M. Adaptive Fractional-Order Nonsingular Fast Terminal Sliding Mode Based Robust Tracking Control of Quadrotor UAV With Gaussian Random Disturbances and Uncertainties. *IEEE Trans. Aerosp. Electron. Syst.* **2021**, *57*, 2265–2277. [CrossRef]
38. Anjum, Z.; Guo, Y.; Yao, W. Fault tolerant control for robotic manipulator using fractional-order backstepping fast terminal sliding mode control. *Trans. Inst. Meas. Control* **2021**, *43*, 3244–3254. [CrossRef]
39. Le, A.T. Neural Observer and Adaptive Fractional-Order Backstepping Fast-Terminal Sliding-Mode Control of RTG Cranes. *IEEE Trans. Ind. Electron.* **2020**, *68*, 434–442.
40. Zhang, W. Research on Permanent Magnet Synchronous Motor Control Based on Fractional Order Sliding Mode Observer. Master's Thesis, Lanzhou Jiaotong University, Lanzhou, China, 2019.

41. Wu, Z. *Hydraulic Control System*, 1st ed.; Higher Education Press: Beijing, China, 2008; pp. 14–43.
42. Shao, X. Research on Position Tracking Control of MDF Continuous Hot Press Plate Thickness Control Hydraulic System. Master's Thesis, Northeast Forestry University, Harbin, China, 2015.
43. Wang, H.; Lu, Y.; Tian, Y.; Christov, N. Fuzzy sliding mode based active disturbance rejection control for active suspension system. *Proc. Inst. Mech. Eng. Part D J. Automob. Eng.* **2020**, *234*, 449–457. [CrossRef]